Supporting Information

Vijayan and Kopell 10.1073/pnas.1215385109

SI Note 1: Muscarinic Acetylcholine Receptor Model Properties

Metabotropic cholinergic agonists are thought to hyperpolarize reticular (RE) cells by increasing their potassium leak conductances (1); they are thought to depolarize thalamocortical (TC) cells by decreasing their potassium leak conductances (2). To mimic the effects of muscarinic acetylcholine receptor (mAChR) agonists we set $\bar{g}_{KL}$ of TC cells to 0.0028 mS/cm^2, so that the TC cells had a depolarized resting membrane potential (∼−60 mV), as is the case during mAChR agonist-induced alpha oscillations (3, 4). Because high-threshold thalamocortical (HTC) cells are thought to be a subtype of TC cells, we assumed that mAChR agonists depolarize HTC cells as well by decreasing their potassium leak conductances. Therefore, we set $\bar{g}_{KL}$ of HTC cells to 0.0069 mS/cm^2, so that the cells had a resting membrane potential of ∼−56 mV; this is within the range of membrane potentials observed in HTC cells during mAChR-induced alpha (3, 4). Note that the HTC cells have additional currents, so $\bar{g}_{KL}$ is not the same for TC cells and HTC cells. The potassium leak conductance of RE cells was set to 0.08 mS/cm^2, resulting in the cells having a relatively hyperpolarized resting membrane potential. An external input to TC cells was provided by a Poisson train of excitatory postsynaptic potentials (EPSPs) (*SI Methods*).

SI Note 2: mGluR1 Model Properties

Metabotropic glutamatergic agonists depolarize both TC cells and RE cells; they are thought to depolarize both cell types by decreasing potassium leak conductances (5, 6). In keeping with these findings, the leak conductances of HTC and TC cells were set to the same values as those in the mAChR model, whereas the leak conductance $\bar{g}_{KL}$ of RE cells was set to 0.005 mS/cm^2, resulting in the RE cells being more depolarized (∼−72 mV) than under the mAChR condition. The resting membrane potentials of TC and HTC cells are the same as under the mAChR condition, ∼−60 mV and −56 mV, respectively. The spiking activity of both thalamic interneurons and RE cells during metabotropic glutamate receptor 1 (mGluR1)-induced alpha is irregular (4), suggesting that the inhibitory drive from both these cell populations onto TC cells is irregular as well. Recall that in our model the indirect inhibition of TC cells by HTC cells via thalamic interneurons is replaced by direct inhibitory connection. To mimic the arrhythmic drive from the interneurons, only a small random fraction of HTC spikes produced an inhibitory postsynaptic potential (IPSP) in TC cells, and the TC cells received a Poisson train of IPSPs as well (*SI Methods*). To produce irregular activity in RE cells, only a small random fraction of HTC spikes produced an EPSP in RE cells, and the RE cells received a Poisson train of EPSPs as well (*SI Methods*). The low-mGluR1 condition on a background of mAChR is similar to the mAChR condition. However, the leak conductance $\bar{g}_{KL}$ of RE cells was set to 0.072, only 90% of HTC spikes drive RE cells, and only 90% of HTC spikes result in inhibition to TC cells (*SI Methods*).

SI Note 3: Role of Interneurons and RE Cells During mGluR1-Induced Alpha

If only RE cells fire irregularly (*SI Methods*) but the interneurons receive a rhythmic drive from the HTC cells, then TC cells show a preference as to when they fire relative to the alpha oscillation (Fig. S4, *Left*; Rayleigh's test, $P = 6.7 \times 10^{-12}$), and similarly if only the interneurons fire irregularly, but the RE cells receive a rhythmic drive, then TC cells once again show a preference as to when they fire relative to the alpha oscillation (Fig. S4, *Right*; Rayleigh's test, $P = 8.5 \times 10^{-4}$).

SI Note 4: Details of TC Signaling During mAChR-Induced Alpha

We consider how thalamic HTC and TC cells project to the neocortex. The fact that thalamic alpha and alpha in the superficial layers of the neocortex are coherent suggests that HTC cells, which are primarily responsible for thalamic alpha (7), project to the superficial layers of the neocortex, as do thalamic matrix cells. If this is indeed the case, one might expect neocortical multiunit activity to be greatest at the trough of neocortical alpha, because HTC cells fire at the trough of thalamic alpha (multiunit and unit activity, Fig. 5*A*). Bollimunta et al. (8) find exactly this; they find that in the superficial layers of the primary visual cortex, multiunit activity is greater during the trough of cortical alpha than during the peak. By contrast, TC cells are known to project to layer IV of the neocortex. In layer IV, multiunit activity is greatest during the peak of alpha (8) [multiunit and unit activity, Fig. 5*A*]. Thus, it appears that HTC cells and TC cells drive neocortical cells to fire at different phases of neocortical alpha.

SI Methods

Equations Governing Model Neurons. All currents are governed by an instance of the equation

$$I = \bar{g} m^n h^k (V - E_{rev}),$$

where $\bar{g}$ is the maximal conductance, m and h are the activation and inactivation gating variables, respectively, and E_{rev} is the reversal potential. The change in the activation variable is governed by the equation

$$\frac{dm}{dt} = \frac{m_\infty(V) - m(V)}{\tau_m(V)},$$

where m_∞ is the steady-state activation function and τ_m is the time constant of activation. The change in the inactivation variable follows an equation of the same form, where m is replaced by h.

RE cells. The membrane potentials of the RE cells are governed by the equation

$$C\frac{dV_{RE}}{dt} = -I_{Na} - I_K - I_L - I_{KL} - I_{TRE} - I_{GABA_A} - I_{AMPA} + I_{app}$$

Potassium current. The potassium current has four activation gates (n = 4) and no inactivation gates (k = 0). Here,

$$m_\infty(V) = \frac{\alpha_m(V)}{\alpha_m(V) + \beta_m(V)}, \quad \tau_m(V) = \frac{1}{\alpha_m(V) + \beta_m(V)},$$

where

$$\alpha_m(V) = \frac{0.032(15 - V_t)}{\exp((15 - V_t)/5) - 1}, \quad \beta_m(V) = 0.5 \exp((10 - V_t)/40)$$
$$V_t = V_{RE} + 55,$$

and $\bar{g}_k = 10$ mS/cm^2 and $E_k = -100$.

Sodium current. The sodium current has three activation gates and one inactivation gate. Below, α_m, β_m, α_h, and β_h relate to m_∞, τ_m, h_∞, and τ_h in the same fashion as above:

$$\alpha_m(V) = \frac{0.32(13-V_t)}{\exp((13-V_t)/4)-1},\quad \beta_m(V) = \frac{0.28(V_t-40)}{\exp((V_t-40)/5)-1}$$

$$\alpha_h(V) = 0.128((17-V_t)/18),\quad \beta_h(V) = \frac{4}{1+\exp((40-V_t)/5)}$$

$$V_t = V_{RE}+55,$$

and

$$\bar{g}_{Na} = 100\ \text{mS/cm}^2\quad E_{Na} = 50.$$

Leak currents. The leak currents have zero activation and inactivation gates and $E_L = -73$, $E_{KL} = -100$. See *Methods* for the conductance values under mAChR and mGluR1 conditions.

I_T current. The I_{TRE} current has two activation gates and one inactivation gate:

$$m_\infty(V) = \frac{1}{(1+\exp(-(V+52)/7.4)},$$

$$\tau_m(V) = 0.999 + \frac{0.333}{(\exp((V+27)/10)+\exp(-(V+102)/15))}$$

$$h_\infty(V) = \frac{1}{(1+\exp((V+80)/5)},$$

$$\tau_h(V) = 28.307 + \frac{0.333}{(\exp((V+48)/4)+\exp(-(V+407)/50))},$$

The maximal conductance is $\bar{g}_{Ca} = 2.3\ \text{mS/cm}^2$. Here, the reversal potential is determined by the Nernst equation, which depends on the intercellular and extracellular calcium concentration. The extracellular calcium concentration is set to 2mM and the change in the intracellular concentration is determined by the equation

$$[\dot{Ca_i}] = \frac{-10I_{TRE}}{2\times 96,485.3} - \frac{[Ca_i]-0.00024}{5}.$$

The first term must be positive; otherwise it is set to zero.

TC cells.

$$C\frac{dV_{TC}}{dt} = -I_{Na} - I_K - I_L - I_{KL} - I_H - I_{TLT} - I_{GABA_A} - I_{GABA_B} + I_{app}.$$

Sodium current. The sodium current is governed by the same equations used for the sodium current in RE cells, except that $\bar{g}_{Na} = 90\ \text{mS/cm}^2$ and $V_t = V_{TC}+25$.

Potassium current. The potassium current is governed by the same equations used for the potassium current in RE cells, except that

$$\bar{g}_K = 10\ \text{mS/cm}^2\ \text{ and } V_t = V_{TC}+25.$$

Leak currents. Here, $E_L = -70$, $\bar{g}_L = 0.01\ \text{mS/cm}^2$, $E_{KL} = -100$, and $\bar{g}_{KL} = 0.0028\ \text{mS/cm}^2$.

I_T currents. The I_{TLT} current has two activation gates and one inactivation gate.

$$m_\infty(V) = \frac{1}{(1+\exp(-(V+59)/6.2)},$$

$$h_\infty(V) = \frac{1}{(1+\exp((V+83)/4.0)},$$

$$\tau_h(V) = \frac{30.8+(211.4+\exp((V+115.2)/5))/(1+\exp((V+86)/3.2))}{3.737}.$$

The maximal conductance is $\bar{g}_{ca} = 2\ \text{mS/cm}^2$. E_{CA} is calculated in the same fashion as that for IT_{RE}. RE cells do not receive an applied current; however, under mGluR1 conditions they receive a Poisson train of excitatory impulses governed by the equation

$$\text{EPSP} = \exp(T(t)-t)(V-0)),$$

where

$$T(t) = \min\{T_1, T_2, \ldots, T_{n-1}, T_n, \ldots | t < T(t)\}.$$

The difference between the arrival times (T) is an exponentially distributed random variable with a mean of either 10 or 25 ms, depending on the simulation. The EPSP pulses have a duration of 2 ms.

I_h current. The I_h current is calculated as follows:

$$I_h = g_h(o_1 + a(1-c_1-o_1))(V-E_h)$$
$$\dot{o}_1 = 0.0001(1-c_1-o_1) - 0.001((1-p_0)/0.01)$$
$$\dot{p}_0 = 0.0004(1-p_o) - 0.004([Ca]_i/0.0002)^2$$
$$\dot{c}_1 = \beta(V)o_1 - \alpha(V)c_1,$$

where

$$\beta(V) = (1-h_\infty)/\tau_s,\quad \alpha(V) = h_\infty/\tau_s$$
$$\tau_s = 20 + 1000/((\exp((V+71.5)/14.2)) + (\exp(-(V+89)/11.6)))$$
$$h_\infty = 1/(1+\exp((V+75)/5.5))$$
$$E_h = -43,\quad g_h = .1\ \text{mS/cm}^2.$$

We set a to 1 in simulations after experimenting with various values as in Bonjean et al. (9). The calcium dynamics are modeled in the same way as those for RE cells. TC cells do not receive an applied current; however, they receive a Poisson train of excitatory impulses under all conditions. These are governed by the same equations as those used for RE cells. Under mGluR1 conditions they also receive a Poisson train of inhibitory impulses, which are similar to the excitatory impulses except that the reversal potential is set to −85 mV and the strength of the inputs is 1.5 times stronger.

HTC cells.

$$C\frac{dV_{HTC}}{dt} = -I_K - I_{Na} - I_L - I_{KL} - I_H - I_{TLT} - I_{THT} - I_{AHP} - I_{GABA_A} - I_{GABA_B} - I_{GJ} + I_{app}.$$

Potassium current. The potassium current is governed by the same equations used for the potassium current in TC cells.

Sodium current. The sodium current is governed by the same equations used for the sodium current in TC cells.

Leak currents. Here, $E_L = -70$, $\bar{g}_L = 0.01\ \text{mS/cm}^2$, $E_{KL} = -100$, and $\bar{g}_{KL} = 0.0069\ \text{mS/cm}^2$.

I_T currents. Here, I_{TLT} is exactly the same as that for TC cells, whereas I_{THT} has two activation gates and one inactivation gate, where

$$m_\infty(V) = \frac{1}{(1+\exp(-(V+40.1)/3.5)}$$

$$h_\infty(V) = \frac{1}{(1+\exp((V+62.2)/5.5)},$$

$$\tau_h(V) = 0.1483\ \exp(-0.09398V) + 5.284\ \exp(0.008855V).$$

The maximal conductance is $\bar{g}_{ca} = 6\ \text{mS/cm}^2$. The calcium dynamics and E_{CA} are calculated in the same fashion as for I_{TRE} and

I_{TLT}. Here, I_{TLT} and I_{THT} have separate pumps, the idea being that the two channel types might be relatively isolated from one another.

I_h current. Here, we use a shifted version of I_h from Golomb et al. (10), where

$$I_h = g_h r(V - E_h),$$

where

$$\begin{aligned}\dot{r} &= (r_\infty - r)/\tau_s\\ \tau_s &= 20 + 1000/((\exp((V + 56.5)/14.2))\\ &\quad +(\exp(-(V + 74)/11.6)))\\ r_\infty &= 1/(1 + \exp((V + 60)/5.5))\\ E_h &= -40,\ \ g_h = 0.36\ \ \mathrm{mS/cm^2}.\end{aligned}$$

I_{AHP}. I_{AHP} has two activation gates and no inactivation gate:

$$m_\infty(V) = \frac{48[Ca]_i^2}{\left(48[Ca]_i^2 + 0.09\right)}$$

$$\tau_m(V) = \frac{1}{\left(48[Ca]_i^2 + 0.09\right)}$$

$$g_{AHP} = 15\ \ \mathrm{mS/cm^2}.$$

I_{GJ}.

$$I_{GJ} = \bar{g}_e\left(V_{HTC} - V_{post}\right)$$

where $\bar{g}_e = 0.003 - 0.005\ \ \mathrm{mS/cm^2}$ and V_{post} is the membrane potential of the cell that is connected to the HTC cell via a gap junction.

I_{APP}.

$$I_{APP} = N(0, 0.1),$$

where N(0, 0.1) denotes an applied current that is normally distributed with a mean of zero and a variance of 0.1. HTC cells receive an applied current under all circumstances, except for the transient stimuli simulations.

Synaptic currents.

AMPA.

$$\begin{aligned}I_{AMPA} &= \bar{g}_{AMPA}[R](V - E_{AMPA})\\ \frac{d[R]}{dt} &= 0.98[T](1 - [R]) - 0.180[R]\end{aligned}$$

where [T] is the transmitter concentration. When a presynaptic cell spikes, the transmitter concentration instantaneously jumps to 0.5 mM and stays at that value for a duration of 0.3 ms. [R] is the fraction of receptors that are open. $E_{AMPA} = 0$; $g_{AMPA} = 0.42$–$0.70\ \mathrm{mS/cm^2}$. During mGluR1 conditions only 1% of HTC spikes drive RE cells via their AMPA synapses.

$GABA_A$.

$$\begin{aligned}I_{GABA_A} &= \bar{g}_{GABA_A}[R](V - E_{GABA_A})\\ \frac{d[R]}{dt} &= 20[T](1 - [R]) - 0.160[R].\end{aligned}$$

T and R are modeled in the same ways as for AMPA.

$E_{GABA_A} = -85$

$\bar{g}_{GABA_A}(\mathrm{mS/cm^2})$:

$RE - - > RE = 0.7011,\ \ RE - - > HTC = 0.0069,$

$RE - - > TC = 0.1036,\ \ HTC - - > TC = 0.0691.$

When the implicit interneurons are in burst mode, there is a 40-ms delay between an HTC cell spike and the activation of $GABA_A$ receptors on TC cells. During mGluR1 conditions only 1% of HTC spikes drive TC cells via their $GABA_A$ synapses.

$GABA_B$.

$$\begin{aligned}I_{GABA_B} &= \bar{g}_{GABA_B}\left(\frac{[G]^4}{[G]^4 + 100}\right)(V - E_{GABA_B})\\ \frac{d[G]}{dt} &= 0.18[R] - 0.034[G]\\ \frac{d[R]}{dt} &= 0.09[T](1 - [R]) - 0.0012[R].\end{aligned}$$

T and R are modeled in exactly the same ways as for AMPA, and $GABA_A$. Here, [G] is the concentration of activated G protein and

$E_{GABA_B} = -95$

$\bar{g}_{GABA_B}(\mathrm{mS/cm^2})$:

$RE - - > HTC = 0.0138,\ \ RE - - > TC = 0.2073.$

Local Field Potential. To examine how TC cell activity might relate to alpha oscillations, we first needed to determine how to model the local field potential (LFP). The alpha oscillations observed in vitro and in vivo persist in the presence of $GABA_A$, $GABA_B$, NMDA, and AMPA receptor blockers (7); that is, the alpha oscillations are observed even when synaptic currents are blocked. Furthermore, HTC cells fire at the alpha frequency even in the presence of these blockers. The above two observations suggested to us that the activity of HTC cells is primarily responsible for alpha oscillations and led us to model the LFP as a function of the membrane potential of HTC cells:

$$LFP = \frac{1}{N}\sum_{k=1}^{N} - V_{HTC}.$$

In those simulations where we compared the effect on phasing of an increase in the number of HTC cells, the right-hand side was not divided by N.

Phase Calculations. We first band-passed the LFP in the alpha frequency. There were asymmetries in the resulting signal; for a phase window of a fixed length, the time it took the alpha rhythm to traverse that phase window varied depending on the specific phase window chosen. For example, in a given cycle the oscillation might take 20 ms to go from 0 to 90° and 30 ms to go from 90 to 180°. As a result, by chance, there is a greater probability that a given spike will occur between 90 and 180° than between 0 and 90°. To correct for this in our calculations of the phase of the spiking activity relative to the alpha oscillation, we did the following. We first calculated the empirical cumulative distribution function (CDF) of the phases of the LFP. The empirical CDF was used to transform the actual phase distribution of the spiking activity to correct for the asymmetry in the LFP (see ref. 11 for details). All histograms of the spiking activity in relation to the phase of alpha oscillations have undergone this transformation. Significance tests (Rayleigh's test) were performed on these transformed distributions.

Transient Stimuli. For transient stimuli a rectangular current pulse was delivered to TC cells. Under these conditions HTC cells did not receive Gaussian noise, so that the phase of the alpha oscillation at a given time was the same across simulations, making comparisons across conditions easier. Also, TC cells did not receive a Poisson train of EPSPs, so that we could be certain that the elicited spike was generated by the transient stimulus.

Modeling Choices. Note that we have included only $GABA_A$ conductances for the inhibition onto TC cells from the interneurons. The experimental data suggest the $GABA_A$ conductance is of most importance during awake alpha (3, 4). This is probably the case for the inhibitory connections to TC and HTC cells as well. However, the $GABA_B$ connections are known to play an important role in oscillations that occur during sleep in the thalamic circuit being modeled (12). Therefore, inputs from the RE cells to the TC cells include $GABA_B$ as well as $GABA_A$ to constrain our model as well as to allow for future extensions of our model.

There are two separate couplings from the thalamic interneurons to the TC cells. This allows for half the interneurons to be in single-spike mode and the other half to be in burst mode. However, in almost all of the simulations the entire network is in either single-spike mode or burst mode. All simulations were robust with respect to different initial conditions.

1. McCormick DA, Prince DA (1986) ACh induces burst firing in thalamic reticular cells by activating a potassium conductance. *Nature* 319:402–405.
2. McCormick DA, Prince DA (1987) Acetylcholine causes rapid nicotinic excitation in the medial habenula, in vitro. *J Neurosci* 7:742–752.
3. Lörincz ML, Crunelli V, Hughes SW (2008) Cellular dynamics of cholinergically induced alpha (8-13 Hz) rhythms in sensory thalamic nuclei *in vitro*. *J Neurosci* 28:660–671.
4. Lorincz ML, Kékesi KA, Juhász G, Crunelli V, Hughes SW (2009) Temporal framing of thalamic relay-mode firing by phasic inhibition during the alpha rhythm. *Neuron* 63: 683–696.
5. McCormick DA, von Krosigk M (1992) Corticothalamic activation modulates thalamic firing through glutamate "metabotropic" receptors. *Proc Natl Acad Sci USA* 89: 2774–2778.
6. Cox CL, Sherman SM (1999) Glutamate inhibits thalamic reticular neurons. *J Neurosci* 19:6694–6699.
7. Hughes SW, et al. (2004) Synchronized oscillations at alpha and theta frequencies in the lateral geniculate nucleus. *Neuron* 42:253–268.
8. Bollimunta A, Mo J, Schroeder CE, Ding M (2011) Neuronal mechanisms and attentional modulation of corticothalamic α oscillations. *J Neurosci* 31:4935–4943.
9. Bonjean M, et al. (2011) Corticothalamic feedback controls sleep spindle duration in vivo. *J Neurosci* 31:9124–9134.
10. Golomb D, Wang XJ, Rinzel J (1994) Synchronization properties of spindle oscillations in a thalamic reticular nucleus model. *J Neurophysiol* 72:1109–1126.
11. Siapas AG, Lubenov EV, Wilson MA (2005) Prefrontal phase locking to hippocampal theta oscillations. *Neuron* 46:141–151.
12. Destexhe A, Bal T, McCormick DA, Sejnowski TJ (1996) Ionic mechanisms underlying synchronized oscillations and propagating waves in a model of ferret thalamic slices. *J Neurophysiol* 76:2049–2070.

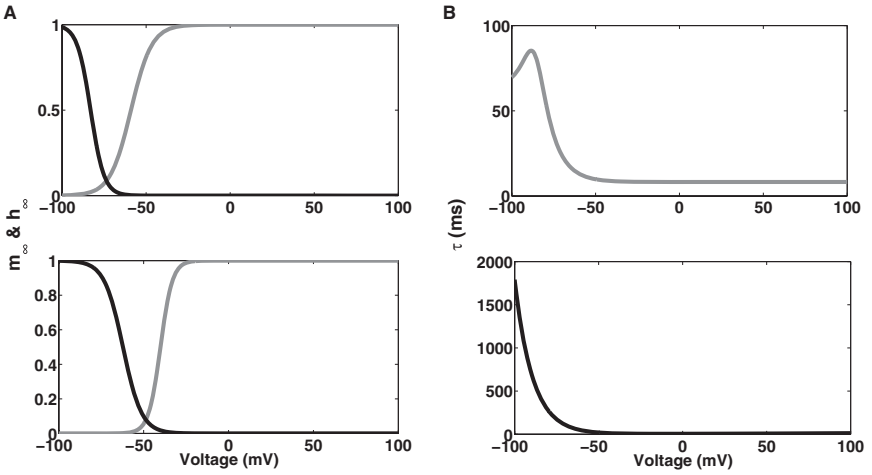

Fig. S1. Activation and inactivation curves of I_{TLT} and I_{THT} channels. (*A*) Activation (m_∞, gray trace, *Upper*) and inactivation (h_∞, black trace, *Upper*) graphs of the standard I_T channel, and activation (m_∞, gray trace, *Lower*) and inactivation (h_∞, black trace, *Lower*) graphs of the I_{THT} channel. (*B*) Graph of the function ($h_\tau(V)$) that determines the time constants of inactivation for the standard I_T channel (*Upper*) and the I_{THT} channel (*Lower*).

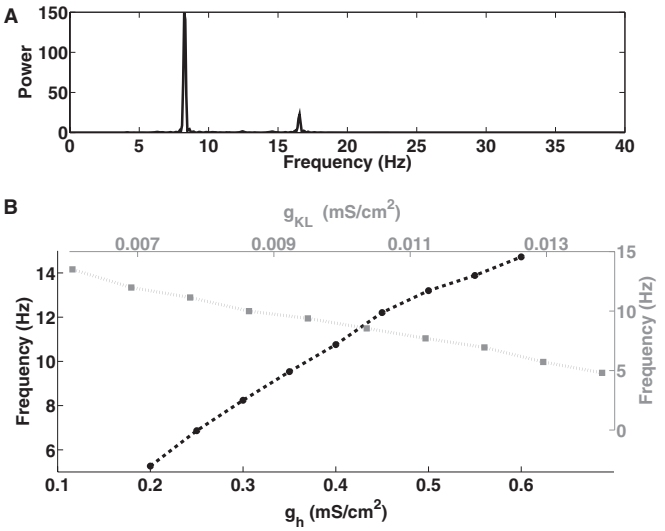

Fig. S2. Glutamergically (mGluR1)-induced alpha. (*A*) Power spectrum of LFP generated in the example shown in Fig. 1*C*. (*B*) Frequency of bursts produced by HTC cells, and therefore frequency of the LFP oscillations, increases as the maximal I_H conductance is increased (black dotted trace and black axes) or as the maximal I_{KL} conductance is decreased (gray trace and gray axes). IT_{HT} channels play the same role in mediating HTBs as their role during mAChR-induced alpha (Fig. 1*E*).

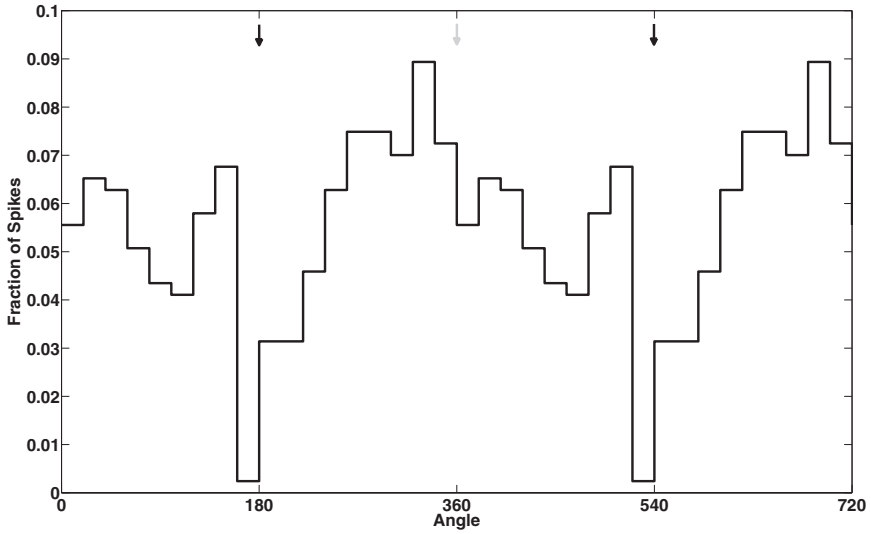

Fig. S3. Cholinergically (mAChR)-induced alpha. Fraction of total spikes that occur at a particular phase of alpha for a single TC cell, during cholinergically (mAChR)-induced alpha with interneurons in burst mode. The *x* axis has been extended to 720°. Black arrows (*Upper*) indicate the angle that corresponds to the peak of the alpha oscillation; gray arrow indicates the angle that corresponds to the trough. Notice that the TC cell tends to fire near the trough of alpha.

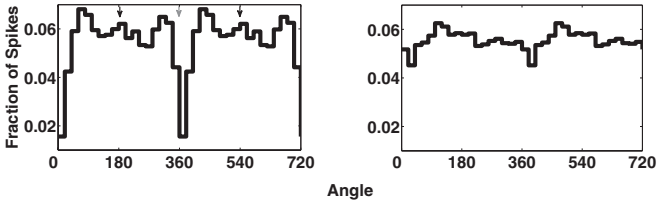

Fig. S4. TC cell activity during mGluR1-induced alpha. (*Left*) TC cell population spiking activity when RE cell activity but not interneuron activity is arrhythmic. Spiking activity is phased (Rayleigh's test, $P = 6.7 \times 10^{-12}$) with cells tending not to fire near the trough of alpha. (*Right*) TC cell population spiking activity when interneuron activity but not RE cell activity is arrhythmic. The spiking activity is phased (Rayleigh's test, $P = 8.5 \times 10^{-4}$), with cells tending not to fire near the trough of alpha.

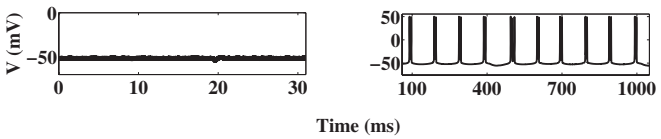

Fig. S5. TC cell activity during low levels of mGluR1 agonists on a background of mAChR agonists. (*Left*) HTC cells are depolarized but quiescent when model parameters aside from the potassium leak conductance are adjusted to reflect the actions of mAChR; the potassium leak conductance (0.0164 mS/cm^2) is greater than in our standard mAChR-induced alpha. (*Right*) With the addition of mGluR1, the leak conductance in the HTC cells is reduced (to 0.0069 mS/cm^2) and the cells begin to oscillate at the alpha frequency.

Table S1. Parameter values

Parameter and condition	RE I_{KL} (mS/cm^2)	RE Poisson train EPSPs	TC Poisson train EPSPs	TC Poisson train IPSPs	HTC I_{KL} (mS/cm^2)	HTC applied current	Interneuron mode	Percentage of implicit interneurons spikes driving TC cells, %	Percentage of HTC spikes driving RE cells, %
mGluR1	0.005	Yes	Yes	Yes	0.0069	N(0,0.1)	Single	1	1
MAChR	0.08	No	Yes	No	0.0069	N(0,0.1)	Single (default); if burst, stated as such	100	100
Background mAChR,No mGluR1 (Fig. S5, *Left*)	0.08	No	Yes	No	0.0164	N(0,0.1)	Single	100	100
Background mAChR, Low mGluR1 (Fig. 4*B* and Fig. S5, *Right*)	0.072	Yes	Yes	Yes	0.0069	N(0,0.1)	Single	90	90
Transient stimuli	0.08	No	No	No	0.0069	No	Single	100	100

Note that the Poisson trains to the TC cells serve as the stimulus in all but the transient stimulus condition.